When faults communicate: Viscoelastic coupling and earthquake clustering in a simple two-fault system

J. C. Lynch, R. Bürgmann, and M. A. Richards
Department of Earth and Planetary Science, University of California, Berkeley, California, USA

R. M. Ferencz
Methods Development Group, Lawrence Livermore National Laboratory, Livermore, California, USA

Received 13 December 2002; accepted 3 February 2003; published 18 March 2003.

[1] 3-D finite element models of a simplified northern and southern San Andreas-type fault system are presented with the goal of better understanding how great earthquakes (M $\geq$ 7.5) on one major segment of a fault can affect the earthquake cycle on another colinear fault segment separated from the first by an asesimically creeping segment. We find that the earthquake cycles of the two seismogenic fault segments become coupled as the lower crustal viscosity and/or the fault separation distance are decreased. Further, models with a 10%–30% difference in relative fault breaking strengths exhibit a bi-modal distribution of repeat times for each fault, resulting in earthquakes that appear clustered in time. *INDEX TERMS:* 8120 Tectonophysics: Dynamics of lithosphere and mantle—general; 8159 Tectonophysics: Rheology—crust and lithosphere; 7260 Seismology: Theory and modeling. **Citation:** Lynch, J. C., R. Bürgmann, M. A. Richards, and R. M. Ferencz, When faults communicate: Viscoelastic coupling and earthquake clustering in a simple two-fault system, *Geophys. Res. Lett.*, *30*(6), 1270, doi:10.1029/2002GL016765, 2003.

1. Introduction

[2] The 1906 San Franciso and the 1857 Ft. Tejon earthquakes mark the last great earthquakes on the northern and southern San Andreas fault (SAF), respectively. Earthquakes of this size (M $\geq$ 7.5) occur on these two fault segments with a repeat time of order 100's of years [*Schwartz et al.*, 2001], and the 1857 and 1906 ruptures account for more than 90% of the total seismic moment released on the SAF in the last 150 years [*Ellsworth*, 1990]. The two rupture segments are separated by a ~170-km-long aseismically slipping section of the SAF. Here we address the question of whether and how great earthquakes on one section of the SAF affect the earthquake cycle of great earthquakes on the other section.

[3] The subject of interacting faults and earthquake triggering has been explored by a number of authors (see *Harris* [1998] for a review). The majority of this work examines changes in the static stress state on one fault due to an earthquake on a nearby fault, and then correlates subsequent earthquakes (or lack thereof) with those changes [e.g., *Stein*, 1999]. Consideration of time-dependent relaxation at depth proved to be important to explain the sequence of the 1999 Hector Mine and 1992 Landers earthquakes [*Freed and Lin*, 2001], and has led to insights regarding the timing of events at Parkfield, CA [*Ben-Zion et al.*, 1993].

[4] Our goal is to explore the simplest model that includes the following first-order properties: 1) far-field tectonic plate velocities drive all deformation in the system; 2) large "northern" and "southern" fault segments only exhibit great earthquakes; 3) a third, smaller fault section connects the northern and southern sections and exhibits no earthquakes, but instead slips continuously with no friction; 4) time-dependent, postseismic deformation is due to the relaxation of a viscoelastic lower crust; and 5) the system is allowed to develop through many earthquake cycles (i.e., thousands of years). The models presented are meant to build our intuition about how such a fault system behaves and how it is affected by slight variations in some of the input parameters.

2. Model Description

[5] We use the commercial finite element package, Spectrum™, developed by Centric Engineering Systems, Inc. (now owned by Ansys, Inc.), to model a long strike-slip fault embedded in a 15-km-thick elastic layer overlying a 35-km-thick viscoelastic layer. The lateral mesh dimensions are 970 km by 670 km (Figure 1). The fault is broken up into three sections: Faults 1 and 2 are 400-km-long sections at each end that slip in great earthquakes but are otherwise no-slip contact surfaces, and these are connected by a freely slipping, 170 km contact surface (labeled "*D*" in Figure 1).

[6] The model is driven by far-field constant velocity boundary conditions imposed on the long edges of the mesh, parallel to the fault, totalling 3.2 cm/yr. To ensure stability of our model calculations and contact for all fault nodes over many earthquake cycles, we constrain the model by imposing no-vertical and no-fault-perpendicular displacement boundary conditions on the top surface and all fault nodes, respectively. While vertical and fault-perpendicular displacements naturally go to zero when averaged over many earthquake cycles, they are part of the full elastic solution for a single slip event in an elastic medium. Numerical calculations with correct boundary conditions show that perturbations in the shear stress relevant to the fault-interaction problem we evaluate are a small fraction (<5%) of the computed stress changes and thus do not significantly affect our results. The solution is quasi-static and each model is run for at least 15,000 model years, of which we focus on the last 5,000 years of the calculation.

0094-8276/03/2002GL016765$05.00

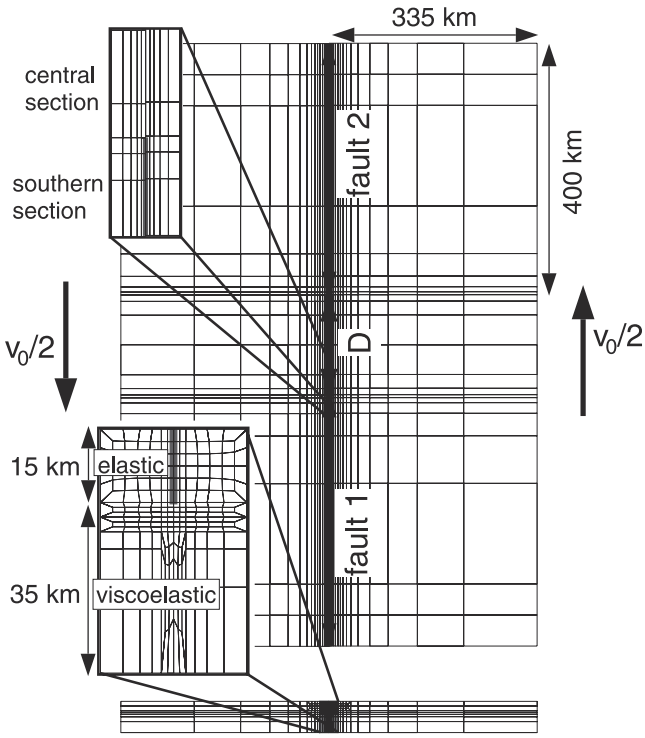

Figure 1. The finite element mesh in map view (above) and cross-section (below). Details of the mesh are shown in the expansions. The contact surfaces that fail in great earthquakes are shaded for clarification. The central section of the fault is a freely slipping contact surface.

The initial 10,000 years of the calculation are necessary for the model to reach a "limit cycle" [*Lyzenga et al.*, 1991; *Lynch and Richards*, 2001].

[7] The two longer faults slip according to a Coulomb-like failure criterion, whereby the average shear stress on both faults is approximated at each time step using the average tangential nodal forces. When this proxy for shear stress exceeds a predetermined threshold value for either fault section, that section slips with no friction for one time step (see *Lynch and Richards* [2001] for a more complete model description). We note that models were also run using a failure criterion determined by the node with the maximum shear stress on each fault, and that this led to model behavior that was virtually identical to the results presented here. The threshold failure criterion was chosen such that the earthquake repeat time would be ~135 years once the model reaches its limit cycle, which is the average repeat time for great earthquakes on the southern SAF [*Sieh et al.*, 1989]. To break the symmetry of the problem, all of the models are initialized by running the first 1000 years with one of the two long faults locked and the other freely slipping, after which the models are restarted with the Coulomb-like failure criterion controlling both faults' behavior.

[8] The Young's modulus, E, and Poisson's ratio, ν, are 75 GPA and 0.25, respectively, for the whole model domain. We vary and examine the effects of three model-parameters: 1) the Maxwell relaxation time, τ, for the lower crust is varied from 0.423 years to 42.3 years, corresponding to Newtonian viscosities, $\eta = \tau E$, of 10^{18} to 10^{20} Pa s (the range of values estimated for California); 2) the separation distance of the two locking faults, D, is varied from 42.5 to 170 km; and 3) the difference in breaking strengths between Fault 1 and Fault 2, ΔS, is varied from 0% to 80% (Table 1).

Table 1. Model Parameters[a]

Model No.	η (Pa s)	D (km)	ΔS
1	10^{19}	170	0%
2	10^{18}	170	0%
3	10^{20}	170	0%
4	10^{19}	85	0%
5	10^{19}	42.5	0%
6	10^{19}	170	10%
7	10^{18}	170	10%
8	10^{19}	170	30%
9	10^{18}	170	30%
10	10^{19}	170	80%

[a] η = lower crustal viscosity, D = fault separation distance, ΔS = percent differential breaking strength.

3. Results

[9] The first two model sets include the reference model (Model 1) and show the effects of lower crustal viscosity (Models 2 and 3), and fault separation distance (Models 4

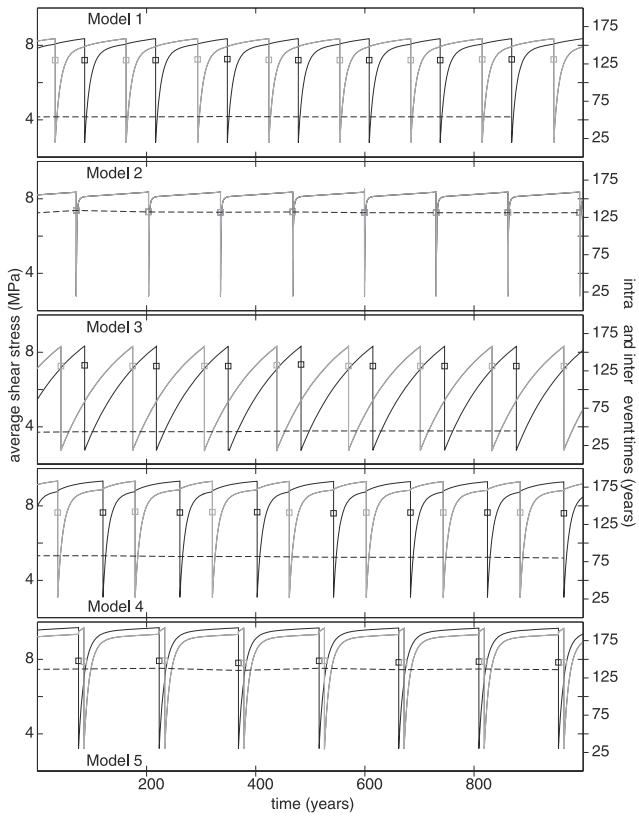

Figure 2. Average shear stress on the two faults is shown (solid and gray lines) with the left y-axis, and intra-event (squares) and inter-event (dashed line) times are shown on the right y-axis, all as a function of time for the last 1000 years of the calculation. The model parameters are described in Table 1.

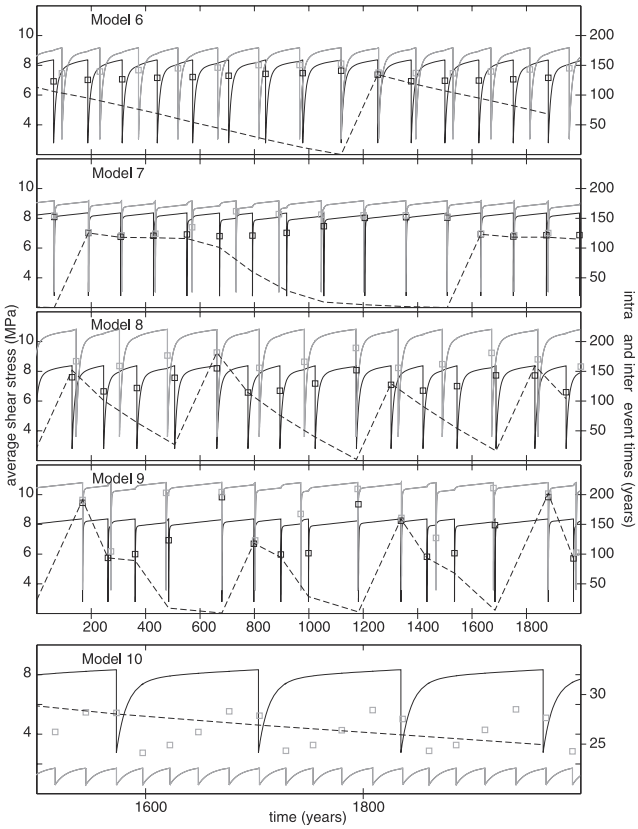

Figure 3. Same as Figure 2, but for Models 6–10. Model numbers refer to Table 1.

and 5). Figure 2 shows the average shear stress on each fault as a function of time for the last 1000 years of the calculation for each of these models. Also shown in Figure 2, on the second y-axis and with the squares, is the repeat time for each earthquake, or intra-event time. The dashed line shows the amount of time between earthquakes on Fault 1 and Fault 2, or the inter-event time.

[10] We note four key features of Models 1–5. 1) The results for the time period shown are essentially identical to the previous 4000 years. The evolution of the shear stress on the fault over time and the inter- and intra-event times are unchanging from one earthquake cycle to the next (i.e., this represents the limit cycle for each model). 2) In comparison to the reference model, lowering the viscosity of the lower crust (Model 2) causes the faults to be reloaded much more quickly, resulting in faults that are closer to their failure threshold throughout their earthquake cycles. In contrast, raising the viscosity (Model 3) leads to faults that are loaded more linearly in time, and thus their proximity to failure at any given time is roughly a linear function of time since the last failure. 3) Coseismic and postseismic effects are seen as discontinuities and changes in slope of the average shear stress curves, respectively, and while difficult to discern in the reference model, these become clearer as the fault separation distance is decreased (Models 4 and 5). 4) Finally, Models 2 and 5 have earthquake ruptures on both faults that occur within a few time steps of each other, indicative of a synchronization of their earthquake cycles (discussed below). It should be noted that these models were re-run with longer initialization periods than the 1000 year period described in section 3, and that this resulted in limit cycles that are indistinguishable from those shown here.

[11] The third set of models addresses the effects of differential fault breaking strengths, or ΔS, on Models 1 and 2 (Figure 3). The graphs in Figure 3 have the same axes as Figure 2 except that the time window is 2000 years for Models 6–9 and 500 years for Model 10. Considering Models 6–9 first, the key features of this model set are: 1) While the time window shown is representative of each model's limit cycle, the loading rate, repeat times and inter-event times change from one earthquake cycle to the next. 2) With $\Delta S = 10\%$ (Models 6 and 7), there are roughly 10 earthquakes on the weaker fault for every 11 earthquakes on the stronger fault, and likewise with $\Delta S = 30\%$ (Models 8 and 9), there are 3 to 4 earthquakes on the weaker fault for every 4 to 5 on the stronger. 3) For $\eta = 10^{18}$ Pa s (Models 7 and 9), there is a tendency for the two faults to fail close in time rather than have events at even time intervals, as evidenced by the inter-event time line alternating between values near zero and the repeat time of Fault 1. For Model 10, with $\Delta S = 80\%$, there are 5 earthquakes on the weaker fault for every earthquake on the stronger fault. The repeat time of Fault 1 is essentially constant (like Models 1–5), and therefore only the repeat time for the weaker fault is shown, which reaches its maximum just before an earthquake on the stronger fault and its minimum after the postseismic relaxation of the stronger fault.

4. Discussion and Conclusions

4.1. The Variability of Repeat Times

[12] We analyze the range of repeat times for Models 6–9 in comparison to Model 1 by means of a normalized histogram of the last 40 events for each fault in Figure 4. For Model 1, the repeat times of 135 years for both faults are unchanging from one earthquake cycle to the next. Changing a fault's breaking strength is analogous to changing its natural earthquake period, so in systems with no communication between faults, we would expect that an

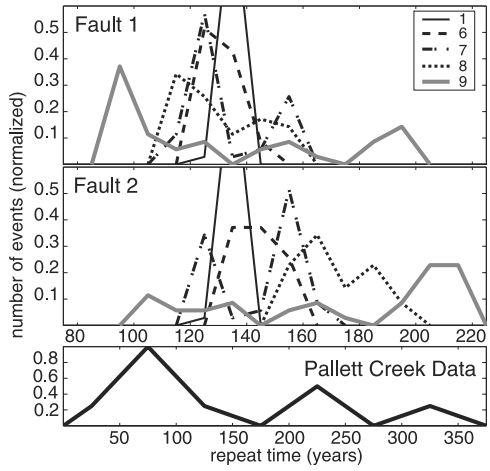

Figure 4. Normalized histograms of repeat times during the last 40 events binned in 10-year intervals for Fault 1 (top panel) and Fault 2 (middle panel). Models 1 and 6–9 are shown. The bottom panel shows data from Pallet Creek, CA, as reported by *Sieh et al.* [1989]. In this data set, 8 events were reported, and these were binned in 50-year intervals.

increase in the breaking strength of one of the faults would mean a shift in its repeat time to a longer period on the histogram. What we see, however, is that a change in breaking strength for one fault not only affects its own repeat time, but also the repeat time of the other fault as well. Specifically, for Model 6, increasing the strength of Fault 2 by 10% shifts its dominant period to ~145, though its range of repeat times is now spread over three histogram bins (from 135 to 155). And though Fault 1's breaking strength is unchanged, its dominant period is decreased to ~125 years and is also spread out over a wider range.

[13] By decreasing the viscosity of the lower crust, the degree of coupling is dramatically increased, as seen in Model 7. Here we see a bi-modal distribution for both faults at periods of 125 years and 155 years, with the stronger fault showing more dominance at the longer period and vice versa for the weaker fault. The strong coupling is also evident in Figure 3 (Model 7), where this distribution of repeat times translates into faults with nearly simultaneous rupture times for many of their cycles.

[14] Increasing the differential breaking strength to 30% again shifts the dominant periods toward wider ranges, with the most striking results seen in Model 9, where Fault 1 has peaks at periods of 95 and 195 years and Fault 2 peaks at 105 and 205–215 years. Again, the natural period of Fault 1 is ~135 years, and with a 30% increase in strength, the expected period of Fault 2 is ~175 years. That both faults have almost no events at their natural periods and instead exhibit repeat times that enable coinciding ruptures is indicative of a strongly coupled system.

[15] If the differential strength is increased still further to 80% (Model 10), the repeat time for Fault 1 is back to its natural period of ~135 years (not shown),while we can see in Figure 3 that the weaker fault exhibits repeat times from 20 to 30 years. In other words, the faults exhibit only one-way (or weak) coupling as the differential breaking strength (or by analogy, differential event sizes) becomes too large.

[16] To summarize, an increase in the breaking strength of a fault leads to longer and, in a non-coupled system, constant repeat times. In coupled systems, however, the "natural" repeat time is only evident by averaging the repeat times of many events. The actual repeat times vary as events on one fault either prematurely trigger events, or relieve stress, causing delayed events. This behavior results in earthquakes that appear clustered in time for either fault.

4.2. Implications for the San Andreas Fault

[17] Models 1–5 build our intuition for how faults communicate in a simple mechanical system, and Models 6–9 show that modest perturbations to this system can lead to fairly complicated behavior. Given that there are numerous important factors in earthquake occurrence that are not considered here (e.g., non-principal events, earthquakes on smaller subsidiary faults, crustal inhomogeneities, etc.), these models suggest that there is little reason to expect earthquakes to happen at regular intervals.

[18] The data set analyzed in the bottom panel of Figure 4 is from Pallett Creek, CA, on the southern SAF near Los Angeles [*Sieh et al.*, 1989], and is one of the more complete records available for a major strike-slip fault. This data set in combination with later work [*Grant and Sieh*, 1994] has led to the suggestion that major earthquakes on the SAF may cluster in time, with several events occuring in relatively quick succession followed by longer periods of quiescence, rather than exhibiting regular repeat times.

[19] While the SAF is undoubtedly a much more complicated system than the models presented here, the Pallett Creek observations appear qualitatively similar to the results of this study. Models that have a moderate difference in breaking strengths between the faults and relatively low viscosity for the lower crust (though within the range thought reasonable for California along the SAF), produce events that appear clustered in time. *Chéry et al.* [2001] showed similar fault interaction effects for models of faults that parallel one another and suggested that postseismic stress transfer could be an important mechanism for such event clusters. Our results are consistant with this conclusion.

[20] Finally, special mention should be made of Model 10. This model has implications similar to the modeling results of *Ben-Zion et al.* [1993], who showed that postseismic relaxation following the 1857 Ft. Tejon earthquake may affect the repeat time of earthquakes at Parkfield, CA (the 1857 earthquake ruptured through the Parkfield segment of the SAF). To expand on that conclusion, our results indicate that even more distant events (i.e., the 1906 San Francisco earthquake) can have a considerable influence on the occurence of Parkfield-type events. Had Model 10 been run with the lower crustal viscosity, this effect would have been even more pronounced.

[21] **Acknowledgments.** This work was performed under the auspices of the U. S. Department of Energy by University of California Lawrence Livermore National Laboratory under contract No.W-7405-Eng-48 and supported by the Institute of Geophysics and Planetary Physics' University Collaborative Research Program under contract 01-GS-007. Berkeley Seismological Laboratory contribution 03-02.

References

Ben-Zion, Y., J. R. Rice, and R. Dmowska, Interaction of the San Andreas Fault creeping segment with adjacent great rupture zones and earthquake recurrence at Parkfield, *J. Geophys. Res.*, *98*, 2135–2144, 1993.

Chéry, J., S. Merkel, and S. Bouissou, A physical basis for time clustering of large earthquakes, *Bull. Seismol. Soc. Am.*, *91*, 1685–1693, 2001.

Ellsworth, W. L., Earthquake history, 1769–1989, in *The San Andreas Fault System*, *California*, edited by R. E. Wallace, chap. 6, *U.S. Geol. Surv. Prof. Pap.*, *1515*, 153–188, 1990.

Freed, A. M., and J. Lin, Hector Mine earthquake by viscoelastic stress transfer, *Nature*, *411*, 180–183, 1999.

Grant, L. B., and K. E. Sieh, Paleoseismic evidence of clustered earthquakes on the San Andreas fault in the Carrizo Plain, California, *J. Geophys. Res.*, *99*, 6819–6841, 1994.

Harris, R. A., Introduction to special section: Stress triggers, stress shadows, and implications for seismic hazard, *J. Geophys. Res.*, *103*, 24,347–24,358, 1998.

Lynch, J. C., and M. A. Richards, Finite element models of stress orientations in well-developed strike-slip fault zones: Implications for the distribution of lower crustal strain, *J. Geophys. Res.*, *106*, 26,707–26,729, 2001.

Lyzenga, G. A., A. Raefsky, and S. G. Mulligan, Models of recurrent strike-slip earthquake cycles and the state of crustal stress, *J. Geophys. Res.*, *96*, 21,623–21,640, 1991.

Sieh, K., M. Stuiver, and D. Brillinger, A more precise chronology of earthquakes produced by the San Andreas fault in southern California, *J. Geophys. Res.*, *94*, 603–623, 1989.

Stein, R. S., The role of stress transfer in earthquake occurence, *Nature*, *375*, 605–609, 1999.

J. C. Lynch, R. Bürgmann, and M. A. Richards, Department of Earth and Planetary Science, University of California, 307 McCone Hall, Berkeley, CA 94720, USA. (lynch@seismo.berkeley.edu)

R. M. Ferencz, Methods Development Group, L-125, Lawrence Livermore National Laboratory, Livermore, CA 94551, USA.